

# Bell-type inequality tests and quantum entanglement from $\Lambda$ -hyperon spin correlations at high energy colliders

Wenjie Gong,<sup>1,\*</sup> Ganesh Parida,<sup>2,†</sup> Zhoudunming Tu,<sup>3,4,‡</sup> and Raju Venugopalan<sup>3,§</sup>

<sup>1</sup>*Department of Physics, Harvard University, Cambridge, Massachusetts 02138*

<sup>2</sup>*Department of Physics, University of Wisconsin-Madison, Madison, Wisconsin 53706*

<sup>3</sup>*Department of Physics, Brookhaven National Laboratory, Upton, NY 11973, USA*

<sup>4</sup>*Center for Frontiers in Nuclear Science, Stony Brook, New York 11794, USA*

(Dated: July 29, 2021)

Spin correlations of  $\Lambda$ -hyperons, extracted from their self-analyzing weak decays, provide unique insight into Bell-type locality tests within the QCD strings formed in high-energy collider experiments. We show from very general considerations that the Clauser-Horne-Shimony-Holt inequality test is typically less stringent for the states produced in QCD strings; however they provide a benchmark for quantum-to-classical transitions induced by varying i) the associated hadron multiplicity, ii) the spin of nucleons, iii) the separation in rapidity between pairs, and iv) the kinematic regimes accessed. These studies also enable the extraction of quantitative measures of quantum entanglement. We explore such questions within a simple model of a QCD string comprised of singlets of two partial distinguishable fermion flavors and compare analytical results to those obtained on quantum hardware. We further discuss a class of spin Hamiltonians that model the complex quantum dynamics of  $\Lambda$  spin correlations embedded in the QCD string. Prospects for extracting quantum information from  $\Lambda$  measurements at current and future colliders are outlined.

Keywords: quantum entanglement, polarization, proton spin structure, CHSH inequality, Electron-Ion Collider

The promise of solving *ab initio* real-time many-body problems in quantum field theory (QFT) motivates the interest in quantum computing for high energy physics [1]. For instance, an outstanding problem in Quantum Chromodynamics (QCD) at high energies is the origin of so-called “ridge” [2] long-range rapidity correlations, which offer unique insight into the thermalization process in the quark-gluon plasma (QGP) [3]. First principles solutions to such open questions in QFT will likely only be obtained well past the noisy intermediate scale quantum (NISQ) era. Nevertheless, focused questions on specific problems universal to simpler systems will provide valuable answers already in the near future [4–20].

For the aforementioned long range phenomenon, such studies may help identify (and classify) its quantum features such as Hanbury-Brown–Twiss and Bose-enhanced gluon correlations [21, 22]. These correlations are a likely consequence of the entanglement of partons (quarks, anti-quarks and gluons) within an ensemble of strings that emerge from the QCD vacuum [23, 24] to stretch in rapidity between the proton fragments; their dynamics underpin Monte Carlo (MC) generators that simulate collider events [25].

An interesting complication results from the quantum correlations of partons not being easily separable from those arising from further rescattering [26] when the

density in a QCD string and the number of strings grows. Can the distinction between the two be understood as a quantum-to-classical transition with increasing multiplicity? Table-top experiments now explore similar questions in cold atomic gases [27]; other examples of this synergy are non-thermal fixed points universal to QGP thermalization and ultracold atomic gases [28, 29].

Further opportunities to isolate quantum correlations within individual QCD strings or small string ensembles exist at electron-positron ( $e^+e^-$ ) colliders [30], in deeply inelastic electron-proton scattering (DIS) experiments [31, 32], and in hadronic collisions [33]. These experiments can address outstanding puzzles such as whether the apparent thermal distribution of small numbers of produced particles could arise from quantum entanglement in a QCD string [34, 35].

In this Letter, we will explore the possibility that  $\Lambda$  and  $\bar{\Lambda}$  hyperon spin correlations can provide novel insight into intrinsically quantum features of parton dynamics. Such measurements are feasible because the weak decay  $\Lambda \rightarrow \pi^- + p$  allows one to extract the  $\Lambda$ 's (and analogously, that of  $\bar{\Lambda}$ ) spin polarization to be  $\mathbf{P} = \alpha \hat{\mathbf{a}}$ , where  $\hat{\mathbf{a}}$  denotes the direction of the daughter proton's momentum in the  $\Lambda$  rest frame, and  $\alpha \approx 0.750$  [36]<sup>1</sup>. Indeed, it was suggested<sup>2</sup> forty years ago [41] that extractions of  $\Lambda$ -hyperon spins could be used in Local Hidden Variable Theory (LHVT) tests [42, 43] employing the Clauser-

\* wenjiegong@college.harvard.edu

† parida@wisc.edu

‡ zhoudunming@bnl.gov

§ rajuv@bnl.gov

<sup>1</sup> This value updates that of 0.642 quoted in Ref. [37].

<sup>2</sup> This possibility was further examined in the the context of  $e^+e^-$  collisions [38]; Bell-type tests have also been proposed for top-quark and Higgs measurements at colliders [39, 40].

Horne-Shimony-Holt (CHSH) [44] inequality defined as

$$|E(\hat{\mathbf{a}}, \hat{\mathbf{b}}) - E(\hat{\mathbf{a}}, \hat{\mathbf{b}}')| + |E(\hat{\mathbf{a}}', \hat{\mathbf{b}}) + E(\hat{\mathbf{a}}', \hat{\mathbf{b}}')| \leq 2, \quad (1)$$

where  $E(\hat{\mathbf{a}}, \hat{\mathbf{b}}) = \langle \psi | \hat{\mathbf{a}} \cdot \sigma_1 \hat{\mathbf{b}} \cdot \sigma_2 | \psi \rangle$  with  $\hat{\mathbf{a}}$  and  $\hat{\mathbf{b}}$  corresponding to the momentum directions of the daughter particles<sup>3</sup>. Measured violations<sup>4</sup> of the CHSH inequality would imply a violation of LHVT.

Specifically, the proposed measurement is of a two-particle correlation function (or equivalently a joint probability distribution),

$$\frac{\langle n_{\hat{\mathbf{a}}}, n_{\hat{\mathbf{b}}} \rangle}{\langle n_{\hat{\mathbf{a}}} \rangle \langle n_{\hat{\mathbf{b}}} \rangle} = \frac{P(\hat{\mathbf{a}}, \hat{\mathbf{b}})}{P(\hat{\mathbf{a}})P(\hat{\mathbf{b}})}, \quad (2)$$

where  $n_{\hat{\mathbf{a}}}$  ( $n_{\hat{\mathbf{b}}}$ ) indicates the number of daughter particles with momentum direction  $\hat{\mathbf{a}}$  ( $\hat{\mathbf{b}}$ ) measured in a single event, and  $\langle \dots \rangle$  denotes the ensemble average. The count pair in the numerator is from the same event; those in the denominator are from different events.

We will first discuss a theorem that encompasses how non-locality and entanglement manifest in Eq. (2). For simplicity, we consider spins in the  $x$ - $z$  plane of the Bloch sphere and assume  $|\mathbf{P}| = 1$ , indicating perfect discrimination between spin-up and spin-down. Thus a daughter proton (or pion) decaying along  $\hat{\mathbf{a}}$  signifies a parent hyperon spin state of spin-up along  $\hat{\mathbf{a}}$ .

The general spin state of the two spin- $\frac{1}{2}$  hyperons (with angles  $\theta_a$  ( $\theta_b$ ) of spin-directions  $\hat{\mathbf{a}}$  ( $\hat{\mathbf{b}}$ ) relative to the  $z$ -axis of the system can be represented by a density matrix  $\rho_{ab} = \sum_{i=1}^4 \sum_{j=1}^4 \lambda_{ij} |B_i\rangle \langle B_j|$  in the Bell basis,

$$\begin{aligned} |B_1\rangle &= \frac{|00\rangle + |11\rangle}{\sqrt{2}}; & |B_2\rangle &= \frac{|00\rangle - |11\rangle}{\sqrt{2}}; \\ |B_3\rangle &= \frac{|01\rangle + |10\rangle}{\sqrt{2}}; & |B_4\rangle &= \frac{|01\rangle - |10\rangle}{\sqrt{2}}, \end{aligned} \quad (3)$$

with  $\lambda_{ij}$  real due to spins being in the  $x$ - $z$  plane. Computing  $P(\hat{\mathbf{a}}, \hat{\mathbf{b}}) = \text{Tr}(|\theta_a\rangle \langle \theta_b| \langle \theta_a| \langle \theta_b| \rho_{ab})$  and likewise,  $P(\hat{\mathbf{a}}) = \text{Tr}(|\theta_a\rangle \langle \theta_a| \rho_a)$ , with  $\rho_a = \text{Tr}_b(\rho_{ab})$ , and assuming both probabilities only depend on  $\theta_a - \theta_b$  (rotational invariance, which sets  $\lambda_{22} = \lambda_{33}$ ), and  $P(\hat{\mathbf{a}}, \hat{\mathbf{b}}) = P(\hat{\mathbf{b}}, \hat{\mathbf{a}})$  (which sets  $\lambda_{ij} = 0$ ,  $i \neq j$ ), we obtain

$$\frac{P(\hat{\mathbf{a}}, \hat{\mathbf{b}})}{P(\hat{\mathbf{a}})P(\hat{\mathbf{b}})} = 1 + (\lambda_{11} - \lambda_{44}) \cos(\theta_a - \theta_b) \quad (4)$$

We therefore conclude,

**Theorem:** *A symmetric, rotationally invariant correlation function implies that the measured state  $\rho_{ab}$*

*is diagonal in the Bell basis, with  $\lambda_{22} = \lambda_{33}$ .*

In the context of the generalized CHSH inequality [48, 49] for mixed two-particle spin- $\frac{1}{2}$  states diagonal in the Bell basis (with  $E(\hat{\mathbf{a}}, \hat{\mathbf{b}}) = E(\theta_a - \theta_b) \equiv E(\theta_{ab})$ , and coplanar spin axes  $\hat{\mathbf{a}}, \hat{\mathbf{a}}', \hat{\mathbf{b}}, \hat{\mathbf{b}}'$ ), Eq. (1) reduces to the one-parameter inequality,

$$\begin{cases} |E(\theta_{ab})| \leq \mathcal{C} \left(1 - \frac{2|\theta_{ab}|}{\pi}\right), & |\theta_{ab}| \leq \frac{\pi}{2} \\ |E(\theta_{ab})| \leq \mathcal{C} \left(1 - \frac{2(\pi - |\theta_{ab}|)}{\pi}\right), & \pi/2 \leq |\theta_{ab}| \leq \pi, \end{cases} \quad (5)$$

where  $\mathcal{C} = |\lambda_{44} - \lambda_{11}|$ . We can obtain  $E(\theta_{ab})$  from the numerator of the measured two-particle correlation function as  $E(\theta_{ab}) = P(\hat{\mathbf{a}}, \hat{\mathbf{b}}) + P(-\hat{\mathbf{a}}, -\hat{\mathbf{b}}) - P(-\hat{\mathbf{a}}, \hat{\mathbf{b}}) - P(\hat{\mathbf{a}}, -\hat{\mathbf{b}})$ , which gives,

$$E(\theta_{ab}) = (\lambda_{11} - \lambda_{44}) \cos(\theta_{ab}). \quad (6)$$

Comparing Eq. (6) to Eq. (5) leads us to a corollary to our Theorem:

**Corollary 1:** *A symmetric, rotationally invariant correlation function implies that the measured state  $\rho_{ab}$  violates its related CHSH inequality, indicating incompatibility with LHVT.*

As the theorem and corollary indicate, the CHSH inequality is violated more easily for mixed states relative to pure states. Since the measured hyperons from a quantum string are likely to be mixed states, the above criteria are sufficient to establish the absence of classical/deterministic explanations of their spin correlations.

One can also quantify entanglement of the  $\Lambda\bar{\Lambda}$  two-particle correlation function in Eq. 4. Of the several discussed in the literature [50], the notion of entanglement fidelity defined as

$$\mathcal{F}_i = \langle B_i | \rho_{ab} | B_i \rangle \equiv \lambda_{ii}, \quad (7)$$

is the most straightforward to extract from measured  $\Lambda\bar{\Lambda}$  spin correlations with  $\rho_{ab}$  entangled if  $\mathcal{F}_i > \frac{1}{2}$ . Since the coefficient of  $\cos(\theta_{ab})$  in Eq. 4 is  $\lambda_{11} - \lambda_{44}$ , we obtain a second corollary to our theorem,

**Corollary 2:** *If the magnitude of the coefficient of  $\cos(\theta_{ab})$  in a symmetric rotationally invariant correlation function is greater than  $\frac{1}{2}$ , then the measured state  $\rho_{ab}$  is entangled.*

We note that  $\mathcal{F}_i > \frac{1}{2}$  is a sufficient but not necessary criterion for entanglement. An entanglement measure that is necessary and sufficient, if more challenging to extract at colliders, is the Peres-Horodecki Positive Partial Transpose (PPT) criterion [51, 52]. This criterion, and its possible measurement, is discussed further in Appendix A.

Following our very general considerations of the CHSH inequality, and entanglement, for mixed states, we will apply these to a very simple spin model for  $\Lambda$ -hyperons embedded in a QCD string. Here strange-anti-strange quarks ( $s\bar{s}$ ) are mixed up with quark pairs of one other

<sup>3</sup> Note that the Pauli operator  $\sigma_i$  acts on particle  $i$ , and we denote spin-up as 1 and spin-down as -1.

<sup>4</sup> Extensive tests of Bell-type inequalities in atomic, molecular, and optical physics experiments show consistent violations despite concerted efforts to devise loopholes [45–47].

flavor  $u\bar{u}$  along the QCD string. This ensemble of  $s, \bar{s}, u$  and  $\bar{u}$  can be thought of as being grouped, after hadronization, into spin singlets with the possible singlet combinations<sup>5</sup> being  $s\bar{s}$ ,  $u\bar{s}$ ,  $s\bar{u}$  and  $u\bar{u}$ . For  $N$  partons in the string, there are  $a$  singlets of type  $s\bar{s}$ ,  $b/2$  singlets of type  $s\bar{u}$ ,  $b/2$  singlets of type  $u\bar{s}$ , and  $N/2 - a - b$  singlets of type  $u\bar{u}$ . This implies that there are  $2a + b$  particles of type  $s$  or  $\bar{s}$  and  $N - 2a - b$  particles of type  $u$  or  $\bar{u}$ . We assume the ground state wavefunction for this state corresponds to these particles occupying the lowest  $N/2$  levels of a system, with  $s\bar{s}$  on levels  $1\dots a$ ,  $s\bar{u}$  on levels  $a + 1\dots a + b/2$ ,  $u\bar{s}$  on levels  $a + b/2 + 1\dots a + b$ , and  $u\bar{u}$  on levels  $a + b + 1\dots N/2$ ; the only relevant aspect of this ground state for us is that the individual wavefunctions are orthogonal.

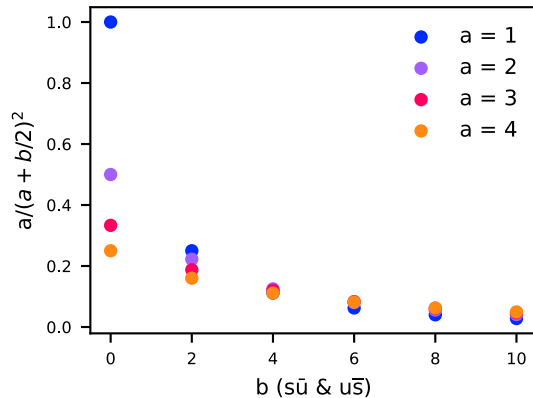


FIG. 1. The coefficient  $\frac{a}{(a+b/2)^2}$  in Eq. (8) plotted for various  $a$  and  $b$  corresponding to  $s\bar{s}$  and  $u\bar{s}(s\bar{u})$  pairs in the string. A coefficient greater than  $\frac{1}{2}$  satisfies the entanglement fidelity criterion.

The explicit computation of  $s\bar{s}$ ,  $s\bar{u}$  and  $u\bar{u}$  correlations in this system is worked out in Appendix B; for the  $s\bar{s}$  ( $\Lambda\bar{\Lambda}$ ) correlations, one obtains the spin correlation function to be,

$$\frac{P(|\hat{n}_1\rangle, |\hat{n}_2\rangle)}{P(|\hat{n}_1\rangle)P(|\hat{n}_2\rangle)} = 1 - \frac{a}{(a+b/2)^2} \cos(\theta_2 - \theta_1). \quad (8)$$

This result, which clearly violates the CHSH inequality, depends only on  $a$  and  $b$  since they are the only parameters that determine the number of  $s\bar{s}$ ,  $s\bar{u}$ , and  $u\bar{s}$  singlets. The coefficient on the cosine is plotted for various  $a$  and  $b$  in Fig. 1. We see that, as may be anticipated, adding mixed singlets, or having  $b > 0$ , decreases the entanglement fidelity since their indistinguishability washes out the spin correlation. The PPT entanglement criterion for this model is discussed in Appendix A.

Our toy model is useful because, even without complex dynamics, it provides analytical insight into the CHSH

inequality and allows us to gauge the relevance of entanglement measures. For example, one could examine what experimental observables could isolate  $\lambda_{11}$  from  $\lambda_{44}$  in the correlation function.

We will now discuss more realistic models of the QCD string and in particular, strings that decay into  $\Lambda\bar{\Lambda}$  pairs. A good starting point for our discussion is the Anderson model of localized impurities coupled to delocalized fermion spins [53],

$$H_{\text{Anderson}} = \sum_{k\sigma} \epsilon_k a_{k\sigma}^\dagger a_{k\sigma} + \epsilon_d d_\sigma^\dagger d_\sigma + U d_\uparrow^\dagger d_\uparrow d_\downarrow^\dagger d_\downarrow + \frac{\eta}{\sqrt{V}} \left( d_\sigma^\dagger a_{k\sigma} + a_{k\sigma}^\dagger d_\sigma \right). \quad (9)$$

Here the  $d_\sigma^\dagger(d_\sigma)$ 's denote the localized impurities with spins  $\sigma$  (denoting heavy strange quarks, which likely carry the spin of the  $\Lambda$ 's [54, 55]) and the  $a_\sigma^\dagger(a_\sigma)$ 's represent the delocalized fermions (light up and down quarks); the first two terms in the Hamiltonian are their respective kinetic energies. The third term is a Hubbard-type hopping term for the light quarks and the final term is the spin coupling between these delocalized fermions and the heavy strange quark impurities. This last term “screens” the formation of  $\Lambda\bar{\Lambda}$  singlets. As is well-known, a Schrieffer-Wolff transformation [56], with the impurity kinetic energy  $\epsilon_d$  below the Fermi energy recovers the Kondo Hamiltonian, wherein the net spin coupling of the delocalized fermions couples to the impurity spin  $\mathbf{S}$ .

Further insight into correlations between the  $\Lambda\bar{\Lambda}$  pairs “doping” the QCD string can be obtained in an extension of the Kondo model<sup>6</sup>, where the ground state includes a filled Fermi sea of light fermions and several impurities, with additional phase factors denoting their spatial locations. Eliminating excitations of the Fermi sea via another Schrieffer-Wolff transformation results in an effective Hamiltonian of localized impurities with interactions mediated by the exchange of virtual electron-hole pairs. The relevant analogy of this RKKY (Ruderman-Kittel-Kasuya-Yoshida) effective Hamiltonian [58–60] to our case is the QCD string at small Bjorken  $x$ , where a large multiplicity of gluons/light quark-antiquark pairs screen the correlations between  $\Lambda$ -hyperons. The RKKY Hamiltonian takes the form

$$H_{\text{RKKY}} = \sum_{jj'} \mathbf{S}_j \cdot \mathbf{S}_{j'} J_{\text{RKKY}}(R_j - R_{j'}), \quad (10)$$

with

$$J_{\text{RKKY}}(R) = \frac{-J^2}{(k_F R)^4} [\sin(2k_F R) - 2k_F R \cos(2k_F R)],$$

where  $k_F$  is the Fermi momentum. This Hamiltonian is

<sup>5</sup> These are proxies for  $\Lambda\bar{\Lambda}$ , kaon and pion states, respectively; up and down quark pairs are taken as indistinguishable.

<sup>6</sup> See [57] for a similar discussion of heavy flavor impurities in quark matter at high baryon densities.

ferromagnetic at short distances but has alternating sign at larger distances, suggestive of glassy dynamics.

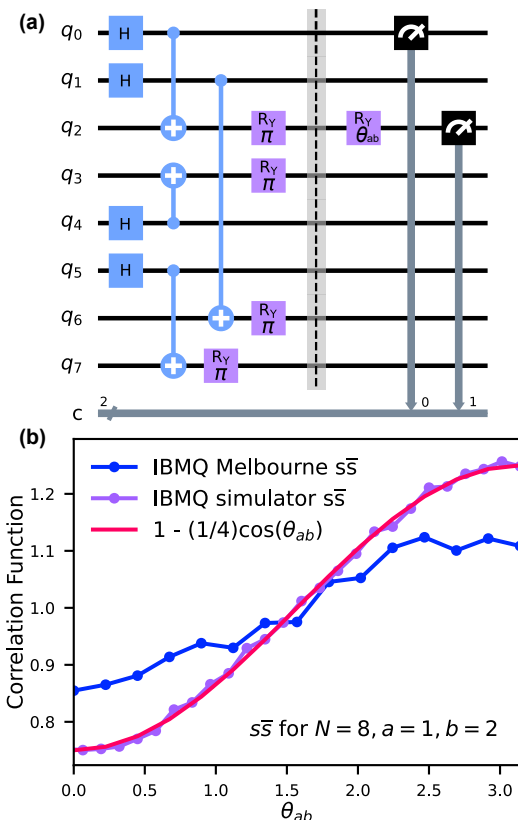


FIG. 2. (a) One of 16 circuits necessary to initialize and simulate the state of  $N = 8$  particles with  $a = 1$   $s\bar{s}$  singlets,  $b = 2$   $s\bar{u}$  and  $u\bar{s}$  singlets and one  $u\bar{u}$  singlet. The barrier separates initialization from simulation of the correlation function. (b) Quantum simulation results for the  $s\bar{s}$  correlation function. The analytical prediction (Eq. 8), is indicated for comparison.

While the RKKY model is a good model of  $\Lambda\bar{\Lambda}$  correlations at small Bjorken  $x$ , a better fit to understand the dynamics of the “impurity doped” QCD string at large Bjorken  $x$  is the Anderson model with multiple impurities [61]. In analogy to a quantum phase transition proposed [62] between Kondo and RKKY regimes, it would be interesting to investigate similar observable consequences of the increased multiplicity of QCD strings with decreasing Bjorken  $x$ . In polarized DIS, valence quark spin plays an analogous role to a magnetic field, providing an additional handle on simulating string dynamics in these spin models.

There are several classical approaches to simulating the ground state properties of the aforementioned spin Hamiltonians [61, 63–66]. However such Hamiltonians suffer from a severe dynamical sign problem that afflicts the extraction of real-time correlations [67]. Since the formation, evolution, and fragmentation of QCD strings are dynamical real-time problems, they are susceptible to the sign problem even in lower dimensional incarnations.

Quantum computers don’t suffer from this problem, and such computations have been performed for the Ising model in an external magnetic field [68]. The Quantum computation of Anderson and Kondo lattices has been discussed previously [69]; digital simulations of these Hamiltonians, adapted to the QCD string, are in progress.

As a first step towards this goal, we have written down quantum circuits for the toy model we outlined and performed computations on IBM’s Qiskit quantum simulator [70] and on IBM Q quantum hardware, specifically `ibmq_16_melbourne` containing 14 qubits. This computation is outlined in Appendix C. In Fig. 2 (a), we show one of the 16 circuits necessary to generate and simulate the mixed spin density matrix for the case of  $N = 8$  spin-1/2 fermions, with  $a = 1$  (one  $s\bar{s}$  pair),  $b = 2$  (one  $s\bar{u}$  and  $\bar{s}u$  singlet each) and  $N/2 - a - b$ , one  $u\bar{u}$  singlet. In Fig. 2 (b), we show the analytical result from Eq. 8 for this case compared to the result from the Qiskit simulator, for which we find good agreement. In contrast, the agreement with actual quantum hardware is not good, illustrating the challenge of reliable quantum simulation in the NISQ era. Our model therefore provides a testing ground for quantum error correction codes prior to quantum simulations of QCD string Hamiltonians.

We consider finally the experimental challenges in measuring  $\Lambda\bar{\Lambda}$  correlations at colliders. The  $\Lambda$  and  $\bar{\Lambda}$

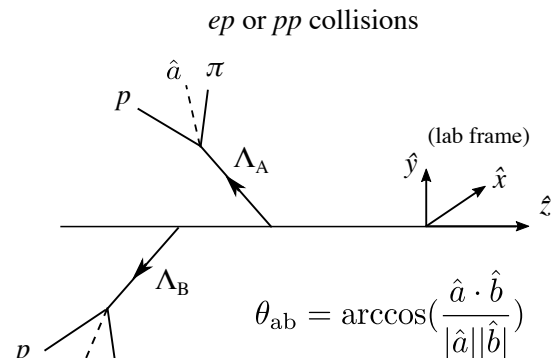


FIG. 3. Illustration of double  $\Lambda$  polarization; here  $\hat{a}$  ( $\hat{b}$ ) denotes the momentum direction of  $\Lambda_A$  ( $\Lambda_B$ ) daughter particle in the  $\Lambda_A$  ( $\Lambda_B$ ) rest frame.

spins are measured in terms of their polarization, where the decay kinematics on an event-averaged basis reflects their spin projections [71–84]. The CHSH inequality and entanglement measures can be extracted from the correlation of their relative spin projections, illustrated in Fig. 3, written as  $\frac{dN}{d\cos(\theta_{ab})} \propto 1 + \alpha^2 P_{\Lambda,\Lambda} \cos(\theta_{ab})$ . As noted, the hyperon decay parameter  $\alpha = 0.750 \pm 0.010$  [36] and  $\theta_{ab}$  is the relative angle between the two daughter particles in their respective mother’s rest frame. A nonzero  $P_{\Lambda,\Lambda}$  implies a spin correlation between the two particles, which can be further directly related to the entanglement fidelity in our model; note that the

cosine modulations in Eq. 8 and in  $\Lambda$ 's weak decay are of different origin.

Currently, no MC generators implement the physics of spin entanglement at the parton level, providing a clear (null result) experimental baseline for spin entanglement searches. Specifically, we can simulate “by hand” spin entanglement in the PYTHIA 8 MC event generator [85]; simulation results and challenges posed for measurements are discussed in Appendix D.

In summary, we have outlined in this Letter theoretical models and experimental signatures of the quantum properties of QCD strings that can be uncovered by  $\Lambda\bar{\Lambda}$  correlation measurements at colliders. The prospects for CHSH tests and entanglement measures were considered both on general grounds and within a specific model. We discussed the scaling up in complexity of theory models towards simulating QCD string properties. First simulations on quantum hardware provide a useful benchmark and illustrate current challenges in reliable extraction of physics. Further systematic studies implementing quantum error correction, state preparation, Trotter evolution, and entanglement measures, will be reported separately. In parallel, MC simulations are in progress studying the potential  $\Lambda$  correlation measurements of the entanglement signatures sketched in Appendix A.

## ACKNOWLEDGMENTS

We thank Robert Konik for discussions on spin Hamiltonians, Elke-Caroline Aschenauer for discussions on spin polarization measurements and Alexander Jentsch for discussions of  $\Lambda$  particle detection in the Far-Forward region at the EIC.

The work of W.G. is supported in part by the U.S. Department of Energy, Office of Science, Office of Workforce Development for Teachers and Scientists (WDTS) under the Science Undergraduate Laboratory Internships Program (SULI). Access to IBM's quantum hardware is provided through Harvard University and Brookhaven National Laboratory's Scientific Data and Computing Center (SDCC) along with the Co-design Center for Quantum Advantage (C<sup>2</sup>QA).

G.P.'s work was supported in part by the S.N. Bose Scholars Program, jointly funded by the Government of India (Department of Science and Technology (DST) - Science & Engineering Board (SERB)), Indo-U.S. Science and Technology Forum (IUSSTF) and WINStep Forward and in part by the U.S. Department of Energy under Award under contract number DE-SC0012704.

The work of Z. Tu is supported by LDRD-039 and the Goldhaber Distinguished Fellowship at Brookhaven National Laboratory. Z. Tu and R.V are supported by the U.S. Department of Energy under the Award under contract number DE-SC0012704.

R.V's work on quantum information science is

supported in part by the U.S. Department of Energy, Office of Science National Quantum Information Science Research Center's Co-design Center for Quantum Advantage (C<sup>2</sup>QA) under contract number DE-SC0012704.

## Appendix A: PPT measure for QCD strings

For mixed states, the Peres-Horodecki criterion [51, 52], also known as the positive partial transpose (PPT) criterion, can be used to detect separability. This criterion is a necessary condition<sup>7</sup> for the separability of the joint density matrix  $\rho$  of two systems  $A$  and  $B$ . We first describe this criterion and then briefly discuss observables that can signal its violation, indicating bipartite entanglement between  $A$  and  $B$ .

If we have  $\rho$  on  $\mathcal{H}_A \otimes \mathcal{H}_B$ ,

$$\rho = \sum_{ijkl} p_{ijkl}^{ij} |i\rangle \langle j| \otimes |k\rangle \langle l|, \quad (\text{A1})$$

where  $|i\rangle, |j\rangle$  ( $|k\rangle, |l\rangle$ ) label an orthonormal basis for  $A$  ( $B$ ), the partial transpose is defined as follows:

$$\begin{aligned} \rho^{T_B} &= (I \otimes T)\rho \\ &= \sum_{ijkl} p_{ijkl}^{ij} |i\rangle \langle j| \otimes (|k\rangle \langle l|)^T \\ &= \sum_{ijkl} p_{ijkl}^{ij} |i\rangle \langle j| \otimes |l\rangle \langle k|. \end{aligned} \quad (\text{A2})$$

If  $\rho$  is separable, then all the eigenvalues of  $\rho^{T_B}$  are non-negative. If  $\rho^{T_B}$  has one or more negative eigenvalues, then  $\rho$  is entangled.

It is enlightening to first consider this criterion on a Werner state [86], or a two-particle mixed state consisting of maximally entangled and maximally mixed components:

$$\rho_{AB} = p|S_{AB}\rangle \langle S_{AB}| + \frac{(1-p)}{4} I_A \otimes I_B, \quad (\text{A3})$$

$$\rho_A = \frac{1}{2} I_A. \quad (\text{A4})$$

We note that our two-particle reduced density matrix in the two-flavor case, Eq. B7, adopts precisely this form. Then, taking the partial transpose over subspace  $B$ , we find that the eigenvalues of  $\rho_{AB}^{T_B}$  are:

$$\nu_1 = \frac{1+p}{4}; \nu_2 = \frac{1-3p}{4}. \quad (\text{A5})$$

Here  $\nu_1$  has multiplicity 3. Since a negative eigenvalue

<sup>7</sup> It is also sufficient if the dimension of the product space is  $2 \times 2$  or  $2 \times 3$ .

indicates entanglement, we deduce that  $\rho$  is entangled for  $1/3 < p \leq 1$ .

As the two-flavor two-particle reduced density matrix is of the specific form of a Werner state, we see that the condition for entanglement according to PPT here—that the coefficient of the cosine in Eq. 8 be greater than  $\frac{1}{3}$ —is actually less restrictive than that predicted by our general theorem, which requires the coefficient to be greater than  $\frac{1}{2}$ .

We can now question whether accordance with the PPT criterion can be detected via the measurement of observables in a high energy collision. It is important to note here that if  $\rho^{T_B}$  does indeed have negative eigenvalues, then  $\rho^{T_B}$  is not a physical state, and thus the act of partial transposition does not correspond to a physical process. However, for any observable  $\hat{A}$ : [87]

$$\langle \hat{A} \rangle_{\rho^{T_B}} = \langle \hat{A}^{T_B} \rangle_{\rho}. \quad (\text{A6})$$

Thus if we can find a positive operator  $\hat{A}^2$ , with corresponding  $(\hat{A}^2)^{T_B}$ , such that

$$\langle \hat{A}^2 \rangle_{\rho^{T_B}} = \langle (\hat{A}^2)^{T_B} \rangle_{\rho} < 0, \quad (\text{A7})$$

this then indicates that  $\rho^{T_B}$  is not positive; hence  $\rho$  is entangled by the PPT criterion. For two-particle density matrices of the form of the Werner state in Eq. A3, we consider

$$\hat{A} = I_1 \otimes I_2 + \sigma_{1x}\sigma_{2x} - \sigma_{1y}\sigma_{2y} + \sigma_{1z}\sigma_{2z}, \quad (\text{A8})$$

$$\hat{A}^2 = 4I_1 \otimes I_2 - 4(-\sigma_{1x}\sigma_{2x} + \sigma_{1y}\sigma_{2y} - \sigma_{1z}\sigma_{2z}), \quad (\text{A9})$$

$$(\hat{A}^2)^{T_2} = 4I_1 \otimes I_2 - 4(-\sigma_{1x}\sigma_{2x} - \sigma_{1y}\sigma_{2y} - \sigma_{1z}\sigma_{2z}). \quad (\text{A10})$$

For the  $\rho$  given in Eq. A3,

$$\begin{aligned} \langle \hat{A}^2 \rangle_{\rho^{T_B}} &= \langle (\hat{A}^2)^{T_B} \rangle_{\rho} = \text{Tr}((\hat{A}^2)^{T_2} \rho) \\ &= 4 - 4\text{Tr}(3p|S_{AB}\rangle \langle S_{AB}|) = 4 - 12p. \end{aligned} \quad (\text{A11})$$

This becomes negative for  $p > \frac{1}{3}$ , as we expect from our previous work. Again, as the reduced two-particle density matrix in the two-flavor case is a Werner state, using  $\hat{A}$  given in Eq. A8 to assess entanglement via the PPT criterion would also yield that the state is entangled when the coefficient of the cosine in Eq. 8 is greater than  $\frac{1}{3}$ .

## Appendix B: Details of two flavor spin chain model

We provide here details of the computation of the two flavor spin chain model containing four different types of particles:  $s, \bar{s}, u$  and  $\bar{u}$  comprising  $N$  total particles, where there are  $a$  singlets of type  $s\bar{s}$ ,  $b$  singlets of type  $s\bar{u}$  or  $u\bar{s}$ , and  $N/2 - a - b$  singlets of type  $u\bar{u}$ .

We can construct an appropriate wavefunction (antisymmetric under exchange of  $s$  with  $s$ ,  $\bar{s}$  with  $\bar{s}$ ,  $u$  with  $u$ , and  $\bar{u}$  with  $\bar{u}$ ) in which  $s\bar{s}$ ,  $s\bar{u}$ ,  $u\bar{s}$ , and  $u\bar{u}$  are paired into singlets:

$$\begin{aligned} |\Psi\rangle &\sim \sum_{\sigma(s)} \sum_{C(\bar{s})} \sum_{\sigma(u)} \sum_{C(\bar{u})} \text{sgn}(\sigma(s)) \text{sgn}(\sigma(u)) \\ &\times \underbrace{|S_{\sigma(1), C(a+\frac{b}{2}+1)} \dots\rangle}_{a \ s\bar{s}} \underbrace{|S_{\sigma(a+1), C(a+\frac{b}{2}+\frac{N}{2}+1)} \dots\rangle}_{\frac{b}{2} \ s\bar{u}} \\ &\times \underbrace{|S_{C(2a+\frac{b}{2}+1), \sigma(2a+b+1)} \dots\rangle}_{\frac{b}{2} \ \bar{s}u} \underbrace{|S_{\sigma(2a+\frac{3b}{2}+1), C(a+b+\frac{N}{2}+1)} \dots\rangle}_{\frac{N}{2}-a-b \ u\bar{u}} \\ &\times \Phi^+(X), \end{aligned} \quad (\text{B1})$$

with  $X = (\sigma(1), \sigma(a + \frac{b}{2} + 1), \dots, (\sigma(2a + \frac{3b}{2} + 1), \sigma(a + b + \frac{N}{2} + 1))$ . The expression above denotes the sum over permutations of the  $s$  and  $u$  particles, as well as the sum over combinations of the  $\bar{s}$  and  $\bar{u}$  particles. For example, we freely permute particles  $1 \dots a + b/2$ , or the  $s$  particles. However, for the  $a + b/2$  total  $\bar{s}$  particles, we must choose  $\binom{a+b/2}{a}$   $a$  particles to pair with the permuted  $s$  particles, leaving the rest to pair with the permuted  $u$  particles. In this manner, we count all the possible permutations that account for indistinguishable  $s$ ,  $\bar{s}$ ,  $u$ , and  $\bar{u}$  while keeping the required singlet structures.

The  $\Phi^+$  operator completely symmetrizes the spatial wavefunctions across all the pairs  $(\sigma(1), \sigma(a + \frac{b}{2} + 1)) \dots (\sigma(2a + \frac{3b}{2} + 1), \sigma(a + b + \frac{N}{2} + 1)) \dots$  as follows:

$$\begin{aligned} \Phi^+((1, \sigma(a + \frac{b}{2} + 1)) \dots) &\sim \\ &\dots \phi^\alpha(\mathbf{x}_{\sigma(1)}) \phi^\alpha(\mathbf{x}_{\sigma(a+\frac{b}{2}+1)}) \phi^\beta(\mathbf{x}_{\sigma(2)}) \phi^\beta(\mathbf{x}_{\sigma(a+\frac{b}{2}+2)}) \dots \\ &+ \dots \phi^\alpha(\mathbf{x}_{\sigma(2)}) \phi^\alpha(\mathbf{x}_{\sigma(a+\frac{b}{2}+2)}) \phi^\beta(\mathbf{x}_{\sigma(1)}) \phi^\beta(\mathbf{x}_{\sigma(a+\frac{b}{2}+1)}) \dots, \end{aligned} \quad (\text{B2})$$

where the superscripts of the single particle spatial wavefunctions,  $\{\phi^\alpha \mid \alpha \in \{1, 2, \dots, \frac{N}{2}\}\}$ , denote the different pair energy levels. Thus the pairs  $(\sigma(1), \sigma(a + \frac{b}{2} + 1)) \dots (\sigma(2a + \frac{3b}{2} + 1), \sigma(a + b + \frac{N}{2} + 1)) \dots$  all each have an equal probability of occupying any level 1 through  $\frac{N}{2}$ .

The full density matrix of the system is given by  $\rho = |\Psi\rangle \langle \Psi|$ . However since in our simple model we only care about the spin subsystem, we compute the reduced density matrix  $\rho_{\text{spin}}$  by tracing out the spatial degrees of freedom:  $\rho_{\text{spin}} = \text{Tr}_{\text{spatial}}(|\Psi\rangle \langle \Psi|)$ .

If we assume that the spatial wavefunctions are orthogonal,  $\langle \phi^\alpha(\mathbf{x}_i) | \phi^\beta(\mathbf{x}_i) \rangle = 0$  for  $\alpha \neq \beta$ , the symmetrized spatial wavefunctions are then also orthogonal. This allows us to simplify the spin density matrix to

$$\rho_{\text{spin}} = \frac{1}{\mathcal{N}} \sum_{\sigma(s)} \sum_{C(\bar{s})} \sum_{\sigma(u)} \sum_{C(\bar{u})}$$

$$\begin{aligned}
& \times \underbrace{|S_{\sigma(1),C(a+\frac{b}{2}+1)}\cdots\rangle}_{a \ s\bar{s}} \underbrace{\langle S_{\sigma(1),C(a+\frac{b}{2}+1)}\cdots|}_{a \ s\bar{s}} \\
& \times \underbrace{|S_{\sigma(a+1),C(a+\frac{b}{2}+\frac{N}{2}+1)}\cdots\rangle}_{\frac{b}{2} \ s\bar{u}} \underbrace{\langle S_{\sigma(a+1),C(a+\frac{b}{2}+\frac{N}{2}+1)}\cdots|}_{\frac{b}{2} \ s\bar{u}} \\
& \times \underbrace{|S_{C(2a+\frac{b}{2}+1),\sigma(2a+b+1)}\cdots\rangle}_{\frac{b}{2} \ s\bar{u}} \underbrace{\langle S_{C(2a+\frac{b}{2}+1),\sigma(2a+b+1)}\cdots|}_{\frac{b}{2} \ s\bar{u}} \\
& \times \underbrace{|S_{\sigma(2a+\frac{3b}{2}+1),C(a+b+\frac{N}{2}+1)}\cdots\rangle}_{\frac{N}{2}-a-b \ u\bar{u}} \underbrace{\langle S_{\sigma(2a+\frac{3b}{2}+1),C(a+b+\frac{N}{2}+1)}\cdots|}_{\frac{N}{2}-a-b \ u\bar{u}}
\end{aligned} \tag{B3}$$

where the normalization

$$\mathcal{N} = \left(a + \frac{b}{2}\right)! \left(\frac{N}{2} - a - \frac{b}{2}\right)! \binom{a + \frac{b}{2}}{a} \binom{\frac{N}{2} - a - \frac{b}{2}}{\frac{b}{2}}. \tag{B4}$$

To compute  $s\bar{s}$  correlations, we must first compute the reduced density matrix:  $\rho_{1,a+\frac{b}{2}+1} = \text{Tr}_{\text{rest}}(\rho_{\text{spin}})$ . To do so, we consider terms of type  $|S_{1,a+\frac{b}{2}+1}\rangle \langle S_{1,a+\frac{b}{2}+1}|$  and  $|S_{1l}\rangle |S_{a+\frac{b}{2}+1,k}\rangle \langle S_{1l}| \langle S_{a+\frac{b}{2}+1,k}|$ . For  $|S_{1,a+\frac{b}{2}+1}\rangle \langle S_{1,a+\frac{b}{2}+1}|$ , the contribution to the reduced density matrix is

$$\frac{a}{(a + \frac{b}{2})^2} |S_{1,a+\frac{b}{2}+1}\rangle \langle S_{1,a+\frac{b}{2}+1}|. \tag{B5}$$

Likewise, for  $|S_{1l}\rangle |S_{a+\frac{b}{2}+1,k}\rangle \langle S_{1l}| \langle S_{a+\frac{b}{2}+1,k}|$ , the contribution to the reduced density matrix is

$$\frac{(a + \frac{b}{2})^2 - a}{(a + \frac{b}{2})^2} \frac{1}{4} I_1 \otimes I_{a+\frac{b}{2}+1}. \tag{B6}$$

Thus the net contribution to the reduced density matrix is

$$\begin{aligned}
\rho_{1,a+\frac{b}{2}+1} &= \frac{a}{(a + \frac{b}{2})^2} |S_{1,a+\frac{b}{2}+1}\rangle \langle S_{1,a+\frac{b}{2}+1}| \\
&+ \frac{(a + \frac{b}{2})^2 - a}{(a + \frac{b}{2})^2} \frac{1}{4} I_1 \otimes I_{a+\frac{b}{2}+1}.
\end{aligned} \tag{B7}$$

With this, we can calculate the two particle probability,

$$\begin{aligned}
P(|\hat{n}_1\rangle, |\hat{n}_2\rangle) &= \text{Tr}(|\theta_1\theta_2\rangle \langle \theta_1\theta_2| \rho_{1,a+\frac{b}{2}+1}) \\
&= \frac{a}{2(a + \frac{b}{2})^2} \sin\left(\frac{\theta_2 - \theta_1}{2}\right)^2 + \frac{(a + \frac{b}{2})^2 - a}{4(a + \frac{b}{2})^2},
\end{aligned} \tag{B8}$$

where  $|\hat{n}\rangle = |\theta\rangle = \cos(\theta/2) |0\rangle + \sin(\theta/2) |1\rangle$ .

Similarly, the single particle reduced density matrix is

$$\begin{aligned}
\text{Tr}_{a+\frac{b}{2}+1}(\rho_{1,a+\frac{b}{2}+1}) &= \frac{a}{2(a + \frac{b}{2})^2} I_1 + \frac{(a + \frac{b}{2})^2 - a}{2(a + \frac{b}{2})^2} I_1 \\
&= \frac{1}{2} I_1,
\end{aligned} \tag{B9}$$

giving  $P(|\hat{n}_1\rangle) = \frac{1}{2}$ . Thus the correlation function for  $s\bar{s}$  is

$$\frac{P(|\hat{n}_1\rangle, |\hat{n}_2\rangle)}{P(|\hat{n}_1\rangle)P(|\hat{n}_2\rangle)} = 1 - \frac{a}{(a + b/2)^2} \cos(\theta_2 - \theta_1), \tag{B10}$$

which is the result reported in Eq. 8. This result only depends on  $a$  and  $b$ , which makes sense, since  $a$  and  $b$  are the only parameters that determine the number of  $s\bar{s}$ ,  $s\bar{u}$ , and  $u\bar{s}$  singlets.

Using the same procedure, we also calculate the  $s\bar{u}(u\bar{s})$  correlations:

$$\frac{P(|\hat{n}_1\rangle, |\hat{n}_2\rangle)}{P(|\hat{n}_1\rangle)P(|\hat{n}_2\rangle)} = 1 - \frac{b/2}{(a + \frac{b}{2})(\frac{N}{2} - a - \frac{b}{2})} \cos(\theta_2 - \theta_1), \tag{B11}$$

and likewise for  $u\bar{u}$ ,

$$\frac{P(|\hat{n}_1\rangle, |\hat{n}_2\rangle)}{P(|\hat{n}_1\rangle)P(|\hat{n}_2\rangle)} = 1 - \frac{(N/2 - a - b)}{(\frac{N}{2} - a - \frac{b}{2})^2} \cos(\theta_2 - \theta_1). \tag{B12}$$

### Appendix C: Implementing the two flavor spin chain model on quantum hardware

To simulate mixed states  $\rho$  on quantum hardware,

$$\rho = \sum_i p_i |\psi_i\rangle \langle \psi_i|, \tag{C1}$$

we adopt the straightforward approach of initializing and testing each constituent pure state  $|\psi_i\rangle \langle \psi_i|$ , and then weighting the results by their appropriate probabilities  $p_i$ .

As a representative case of the two flavor spin chain model, we specifically consider an ensemble of  $N = 8$  particles, with  $a = 1$   $s\bar{s}$  singlets,  $b = 2$  total  $s\bar{u}$  and  $u\bar{s}$  singlets, and one  $u\bar{u}$  singlet. From Eq. B3, we see that our initial state is then given by the spin density matrix:

$$\begin{aligned}
\rho &= \frac{1}{16} (|S_{13}S_{27}S_{45}S_{68}\rangle \langle S_{13}S_{27}S_{45}S_{68}| \\
&+ |S_{13}S_{27}S_{46}S_{58}\rangle \langle S_{13}S_{27}S_{46}S_{58}| \\
&+ |S_{23}S_{17}S_{45}S_{68}\rangle \langle S_{23}S_{17}S_{45}S_{68}| \\
&+ |S_{23}S_{17}S_{46}S_{58}\rangle \langle S_{23}S_{17}S_{46}S_{58}| \\
&+ |S_{14}S_{27}S_{35}S_{68}\rangle \langle S_{14}S_{27}S_{35}S_{68}| \\
&+ |S_{14}S_{27}S_{36}S_{58}\rangle \langle S_{14}S_{27}S_{36}S_{58}| \\
&+ |S_{24}S_{17}S_{35}S_{68}\rangle \langle S_{24}S_{17}S_{35}S_{68}| \\
&+ |S_{24}S_{17}S_{36}S_{58}\rangle \langle S_{24}S_{17}S_{36}S_{58}| \\
&+ |S_{13}S_{28}S_{45}S_{67}\rangle \langle S_{13}S_{28}S_{45}S_{67}| \\
&+ |S_{13}S_{28}S_{46}S_{57}\rangle \langle S_{13}S_{28}S_{46}S_{57}| \\
&+ |S_{23}S_{18}S_{45}S_{67}\rangle \langle S_{23}S_{18}S_{45}S_{67}| \\
&+ |S_{23}S_{18}S_{46}S_{57}\rangle \langle S_{23}S_{18}S_{46}S_{57}| \\
&+ |S_{14}S_{28}S_{35}S_{67}\rangle \langle S_{14}S_{28}S_{35}S_{67}|
\end{aligned}$$

$$\begin{aligned}
& + |S_{14}S_{28}S_{36}S_{57}\rangle \langle S_{14}S_{28}S_{36}S_{57}| \\
& + |S_{24}S_{18}S_{35}S_{67}\rangle \langle S_{24}S_{18}S_{35}S_{67}| \\
& + |S_{24}S_{18}S_{36}S_{57}\rangle \langle S_{24}S_{18}S_{36}S_{57}|. \quad (\text{C2})
\end{aligned}$$

The initialization of the first term in Eq. C2 on a quantum circuit is shown in Fig. 2(a).

To simulate a correlation function measurement of Eq. 8– the second part of the circuit in Fig. 2(a)– we first select two representative qubits to probe. For  $s\bar{s}$  correlations, we choose qubits  $q_0$ , representing a  $s$  spin, and  $q_2$ , representing a  $\bar{s}$  spin. Note that as the spins are indistinguishable within the same particle type, our particular selection of qubits does not matter. We then rotate one of the selected qubits,  $q_2$  in our case, by a varying  $\theta_{ab}$  about the  $y$  axis, thus demonstrating varying spin polarizations projected into the  $x - z$  plane.

For each  $\theta_{ab}$ , we measure  $q_0$  and  $q_2$  in the  $z$  basis for a total of 1000 shots. The joint probability that both qubits point in the same direction is thus  $n_{11}/1000$ , while the individual probabilities are  $n_{10}/1000$  and  $n_{01}/1000$ , where  $n_{11}$  indicates the counts of the measurement result '11'. For each  $\theta_{ab}$ , we thus see from the general form of the correlation function Eq. 2 that the correlation is

$$1000 \cdot \frac{n_{11}}{n_{10}n_{01}}. \quad (\text{C3})$$

Averaging this across all 16 circuits, each representing a term in Eq. C2, for each  $\theta_{ab}$  value produces the plot in Fig. 2(b).

Though this method of simulating mixed states via constructing pure states and averaging is straightforward, it can be cumbersome and redundant as the same simulation must be run multiple times for a single result. Instead, it is useful to note a mixed state Eq. C1 can also be initialized by constructing the pure state

$$\rho' = \sum_{i=0}^{\mathcal{N}-1} \sqrt{p_i} |\psi_i\rangle |i\rangle. \quad (\text{C4})$$

Here  $\mathcal{N}$  is the total number of terms in the mixed state, and  $i$  counts over the terms in binary. After initializing  $\rho'$ , if we then only work in the subspace spanned by the  $|\psi_i\rangle$ , we effectively have the mixed state Eq. C1. As an example, we can construct our ensemble  $N = 8$ ,  $a = 1$ ,  $b = 2$  using this method. The requisite circuit is given in Fig. 4. For our states, we need a total of  $\log_2(\mathcal{N})$  ancilla initialized in an equal superposition of  $|0\rangle$  to  $|\mathcal{N}\rangle$ . We then perform cSWAP controlled on each of  $i$  on the ancilla,  $i \in [0, \mathcal{N}]$ , targeting the necessary qubits needed to swap from one configuration of permutations to another. Note that though this way of initialization is more concise, it has a much higher cost of multi-qubit gates.

## Appendix D: Measuring $\Lambda\bar{\Lambda}$ correlations at collider energies

The experimental method of measuring  $\Lambda\bar{\Lambda}$  correlation in high energy collisions is similar across all available systems ( $e^+e^-$ ,  $ep$  DIS, and  $pp$  collisions). Therefore we will use  $ep$  DIS to elaborate on the experimental techniques and associated challenges.

Fig. 5 shows two  $\Lambda$  (either  $\Lambda$  or  $\bar{\Lambda}$ ) particles produced in a high energy  $ep$  DIS collision decay into protons and pions. The daughter momentum can be reconstructed using particle detectors and boosted back to the rest frame of the  $\Lambda$  particle, where either daughter particle can be used. In the rest frame of  $\Lambda$ , the momenta vector of the daughter are represented by  $\hat{a}$  and  $\hat{b}$  for  $\Lambda_A$  and  $\Lambda_B$ , respectively. The nature of the weak decay of  $\Lambda$  particle will reflect the  $\Lambda$  spin in terms of the decay angular distribution in the rest frame. In the simplest (albeit unrealistic) scenario, the  $\hat{a}$  and  $\hat{b}$  are the spin directions of  $\Lambda_A$  and  $\Lambda_B$ , which is considered in the model discussed earlier in this Letter. However, in reality, the direction of the decay is smeared by an angular distribution as

$$\frac{dN}{d\cos(\theta^*)} \propto 1 + \alpha P_\Lambda \cos(\theta^*). \quad (\text{D1})$$

Here the hyperon decay parameter  $\alpha = 0.750 \pm 0.010$  [36], and the angle  $\theta^*$  is the angle between the decay daughter and the spin projection axis in the rest frame of  $\Lambda$ .

There are two key aspects to understanding the measurement. First, the spin of the  $\Lambda$  is measured through an angular distribution, and thus not event-by-event accessible. Even if the weak constant is unity and the spin is perfectly aligned with the projected axis, the decay angular distribution is still a cosine modulation with its amplitude at the maximum. It is important to note that this cosine modulation is different from that in Eq. 8, which is a property of CHSH inequality. The underlying correspondence of the two will be investigated in a future study.

Secondly, the weak decay constant sets the maximum measurable modulation of the cosine distribution, and in particular  $\alpha^2 \sim 50\%$  in  $\Lambda\bar{\Lambda}$  correlations because there are two decays involved. Therefore in order to properly compare the experimental data with our model or quantum simulations on a digital quantum computer, the nature of the  $\Lambda$ 's weak decay will have to be taken into account.

In order to validate double  $\Lambda$  polarization, the first step is to check the experimental method in MC generators. We use the PYTHIA 8 Monte Carlo (MC) event generator to simulate the  $ep$  DIS events with  $\Lambda$  particles for kinematic phase space  $1 < Q^2 < 100 \text{ GeV}^2$  and  $0.05 < y < 0.95$ . Here  $Q^2$  is the virtuality of the emitted virtual photon and  $y$  is the inelasticity of the DIS event. A total of 4 billion events are generated, corresponding to an integrated luminosity of  $\sim 3 \text{ fb}^{-1}$ . The energy configuration is chosen at the top energy for

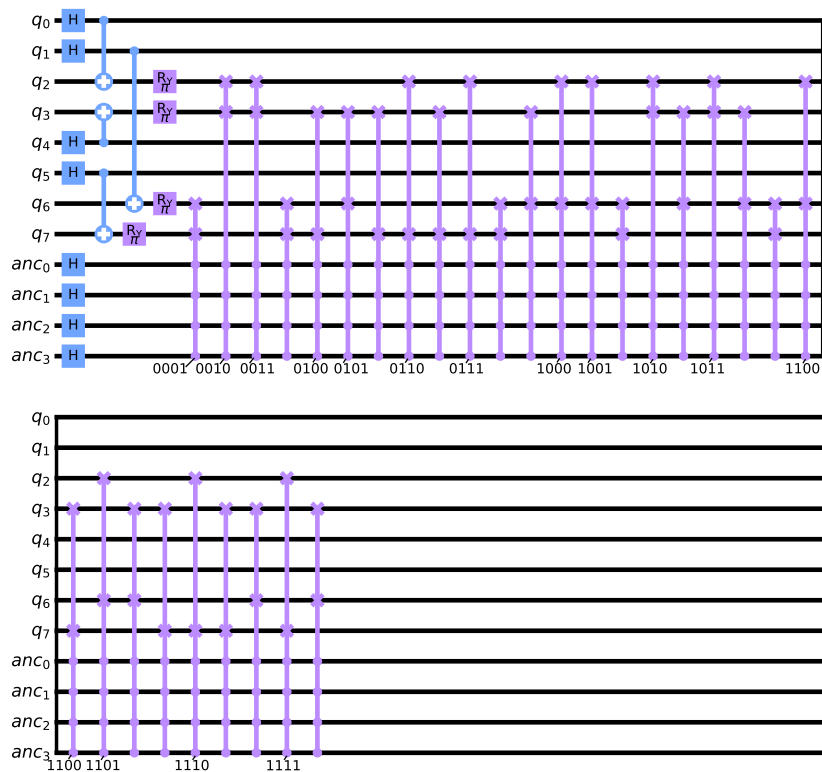


FIG. 4. A circuit that initializes Eq. C2 in the main quantum register. Swaps controlled on each of  $i \in [0, 16]$ , where  $i$  counts in binary, are applied to initialize a full state of the form Eq. C4. The binary form of  $i$  for each group of cSWAPs is listed in the circuit.

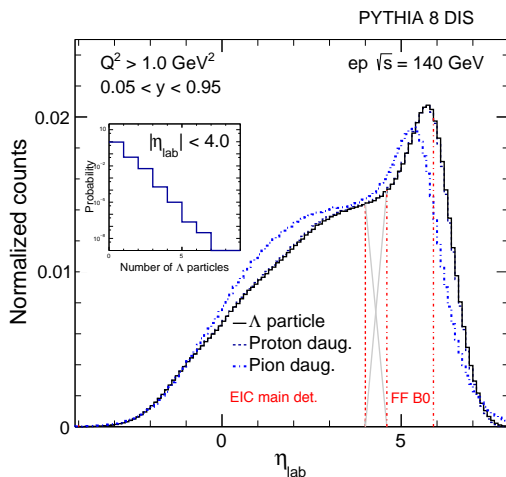


FIG. 5. Pseudorapidity distributions of  $\Lambda$  particles and their decays in  $ep$  DIS events using the PYTHIA 8 model [85]. The acceptance of the EIC main detector and the Far-forward region B0 tracker are shown by the red dashed line. The number of  $\Lambda$  particles per event is also shown.

$ep$  collisions at the Electron-Ion Collider [88]—18 GeV electrons scattering off 275 GeV proton beams. In this study, the detector and beam related effects, for instance the inefficiency of the detector or the angular divergence

of the beam, are not implemented. However a basic detector acceptance is used based on EIC design [89],  $|\eta_{\text{lab}}| < 4.0$  and  $p_T > 150$  MeV, for accepting the  $\Lambda$  particles and their decays in the main detector. In Fig. 5, the pseudorapidity distributions of  $\Lambda$  particles and their decay products in  $ep$  DIS events for center-of-mass energy 140 GeV are shown. The acceptance of the main detector and in the far-forward (FF) region using the B0 tracker (FF B0) is indicated by the red dashed line. In the inset panel, the number of  $\Lambda$  particles is shown per event within the EIC acceptance. Similar measurements can be performed using  $pp$  collisions at Relativistic Heavy-Ion Collider (RHIC) and at the Large Hadron Collider.

In Fig. 6, the default and weighted PYTHIA simulations are shown in terms of the cosine of angular distribution,  $\cos(\theta_{\text{ab}})$ . It is expected that in the default PYTHIA events (upper), the cosine of angular distribution is flat, implying no  $\Lambda\Lambda$  (or  $\Lambda\bar{\Lambda}$ ) spin correlations. However, with an event-weighted sample, where the weight is  $P_{\Lambda,\Lambda} = 50\%$ , the angular asymmetry is then visible. The fitted value of  $P_{\Lambda,\Lambda}$  is consistent with 50% as was put in. The exercise of validating this observable in the PYTHIA event generator is to clearly setup the experimental baseline for such measurement, where no trivial kinematic effect can generate a background in the correlation.

A discussion of the measurement of  $\Lambda\bar{\Lambda}$  correlations

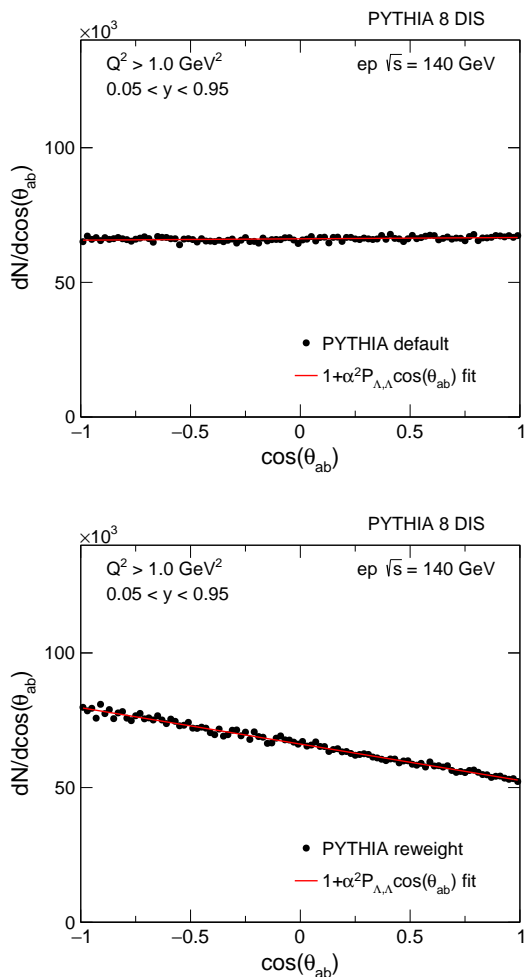


FIG. 6. Upper: the  $\cos(\theta_{ab})$  distribution is plotted for one  $\Lambda$  with respect to the second  $\Lambda$  particle in default PYTHIA 8 [85] simulation. Lower: the same quantity with weighted events, where weights are determined based on polarization value  $P_{\Lambda,\Lambda} = 50\%$ .

in high energy experiments would be remiss without discussing the machine capabilities and experimental challenges. Firstly, the RHIC accelerator (and the upcoming EIC) have the capability of polarizing the target proton or light ions. By polarizing the target, the constituent quarks and gluons can be polarized such that the resulting QCD strings are in different configurations. This is an advantageous experimental handle to control the system, where an asymmetry measurement related to the  $\Lambda\bar{\Lambda}$  correlation could be developed. In addition, the target polarization may provide a specific initial condition for considering the entangled Bell-states and the spin Hamiltonian, which helps data-model comparisons.

In terms of the experiment, the rapidity separation of the two  $\Lambda$  particles is an important quantity for selecting  $\Lambda$ s from different distant scales in a QCD string. Therefore it is essential to have a wide rapidity coverage for the experiment, where widely separated  $\Lambda$  particles can be reconstructed. Without good rapidity coverage, acceptance effects could be difficult and challenging to correct for. Finally, the measurement of  $\Lambda\bar{\Lambda}$  correlations is not only constrained by the  $\Lambda$ 's decay properties, but also detector effects. Given the anticipated small magnitude for the correlation signal, the momentum resolution of daughter particles and the  $\Lambda$  particle will significantly impact the precision of the spin projection. Therefore detectors with high momentum resolution are desirable.

- 
- [1] J. Preskill, Simulating quantum field theory with a quantum computer, *PoS LATTICE2018*, 024 (2018), [arXiv:1811.10085 \[hep-lat\]](#).
- [2] V. Khachatryan *et al.* (CMS), Observation of long-range, near-side angular correlations in proton-proton collisions at the LHC, *JHEP* **09**, 091, [arXiv:1009.4122 \[hep-ex\]](#).
- [3] J. Berges, M. P. Heller, A. Mazeliauskas, and R. Venugopalan, Thermalization in qcd: theoretical approaches, phenomenological applications, and interdisciplinary connections, (2020), [arXiv:2005.12299 \[hep-th\]](#).
- [4] S. R. Beane, D. B. Kaplan, N. Klco, and M. J. Savage, Entanglement Suppression and Emergent Symmetries of Strong Interactions, *Phys. Rev. Lett.* **122**, 102001 (2019), [arXiv:1812.03138 \[nucl-th\]](#).
- [5] N. Mueller, A. Tarasov, and R. Venugopalan, Deeply inelastic scattering structure functions on a hybrid quantum computer, *Phys. Rev. D* **102**, 016007 (2020), [arXiv:1908.07051 \[hep-th\]](#).
- [6] H. Lamm, S. Lawrence, and Y. Yamauchi (NuQS), Parton physics on a quantum computer, *Phys. Rev. Res.* **2**, 013272 (2020), [arXiv:1908.10439 \[hep-lat\]](#).
- [7] B. Chakraborty, M. Honda, T. Izubuchi, Y. Kikuchi, and A. Tomiya, Digital Quantum Simulation of the Schwinger Model with Topological Term via Adiabatic State Preparation, (2020), [arXiv:2001.00485 \[hep-lat\]](#).
- [8] D. E. Kharzeev and Y. Kikuchi, Real-time chiral dynamics from a digital quantum simulation, *Phys. Rev. Res.* **2**, 023342 (2020), [arXiv:2001.00698 \[hep-ph\]](#).
- [9] M. Kreshchuk, W. M. Kirby, G. Goldstein, H. Beauchemin, and P. J. Love, Quantum Simulation of Quantum Field Theory in the Light-Front Formulation, (2020), [arXiv:2002.04016 \[quant-ph\]](#).
- [10] J. Liu and Y. Xin, Quantum simulation of quantum

- field theories as quantum chemistry, *JHEP* **12**, 011, [arXiv:2004.13234 \[hep-th\]](#).
- [11] R. A. Briceño, J. V. Guerrero, M. T. Hansen, and A. M. Sturzu, Role of boundary conditions in quantum computations of scattering observables, *Phys. Rev. D* **103**, 014506 (2021), [arXiv:2007.01155 \[hep-lat\]](#).
- [12] Z. Davoudi, I. Raychowdhury, and A. Shaw, Search for Efficient Formulations for Hamiltonian Simulation of non-Abelian Lattice Gauge Theories, (2020), [arXiv:2009.11802 \[hep-lat\]](#).
- [13] W. A. de Jong, K. Lee, J. Mulligan, M. Płoskoń, F. Ringer, and X. Yao, Quantum simulation of non-equilibrium dynamics and thermalization in the Schwinger model, (2021), [arXiv:2106.08394 \[quant-ph\]](#).
- [14] E. Gustafson, Y. Zhu, P. Dreher, N. M. Linke, and Y. Meurice, Real-time quantum calculations of phase shifts using wave packet time delays, (2021), [arXiv:2103.06848 \[hep-lat\]](#).
- [15] J. a. Barata, N. Mueller, A. Tarasov, and R. Venugopalan, Single-particle digitization strategy for quantum computation of a  $\phi^4$  scalar field theory, *Phys. Rev. A* **103**, 042410 (2021), [arXiv:2012.00020 \[hep-th\]](#).
- [16] J. a. Barata and C. A. Salgado, A quantum strategy to compute the jet quenching parameter  $\hat{q}$ , (2021), [arXiv:2104.04661 \[hep-ph\]](#).
- [17] T. Li, X. Guo, W. K. Lai, X. Liu, E. Wang, H. Xing, D.-B. Zhang, and S.-L. Zhu, Partonic Structure by Quantum Computing, (2021), [arXiv:2106.03865 \[hep-ph\]](#).
- [18] M. Honda, E. Itou, Y. Kikuchi, L. Nagano, and T. Okuda, Digital quantum simulation for screening and confinement in gauge theory with a topological term, (2021), [arXiv:2105.03276 \[hep-lat\]](#).
- [19] K. Ikeda, D. E. Kharzeev, and Y. Kikuchi, Real-time dynamics of Chern-Simons fluctuations near a critical point, *Phys. Rev. D* **103**, L071502 (2021), [arXiv:2012.02926 \[hep-ph\]](#).
- [20] N. Klco and M. J. Savage, Entanglement Spheres and a UV-IR connection in Effective Field Theories, (2021), [arXiv:2103.14999 \[hep-th\]](#).
- [21] A. Dumitru, K. Dusling, F. Gelis, J. Jalilian-Marian, T. Lappi, and R. Venugopalan, The Ridge in proton-proton collisions at the LHC, *Phys. Lett. B* **697**, 21 (2011), [arXiv:1009.5295 \[hep-ph\]](#).
- [22] A. Kovner and V. V. Skokov, Bose enhancement, the Liouville effective action and the high multiplicity tail in p-A collisions, *Phys. Rev. D* **98**, 014004 (2018), [arXiv:1805.09296 \[hep-ph\]](#).
- [23] J. B. Kogut and L. Susskind, Hamiltonian Formulation of Wilson's Lattice Gauge Theories, *Phys. Rev. D* **11**, 395 (1975).
- [24] G. S. Bali, QCD forces and heavy quark bound states, *Phys. Rept.* **343**, 1 (2001), [arXiv:hep-ph/0001312](#).
- [25] B. Andersson, G. Gustafson, G. Ingelman, and T. Sjostrand, Parton Fragmentation and String Dynamics, *Phys. Rept.* **97**, 31 (1983).
- [26] K. Dusling, W. Li, and B. Schenke, Novel collective phenomena in high-energy proton-proton and proton-nucleus collisions, *Int. J. Mod. Phys. E* **25**, 1630002 (2016), [arXiv:1509.07939 \[nucl-ex\]](#).
- [27] B. Luca, M. Holten, R. Klemm, K. Subramanian, J. Bjerlin, S. M. Reimann, G. M. Bruun, P. M. Preiss, and S. Jochim, Observing the emergence of a quantum phase transition shell by shell, *Nature* **587**, 583 (2020), [arXiv:2004.14761 \[cond-mat.quant-gas\]](#).
- [28] J. Berges, K. Boguslavski, S. Schlichting, and R. Venugopalan, Universality far from equilibrium: From superfluid Bose gases to heavy-ion collisions, *Phys. Rev. Lett.* **114**, 061601 (2015), [arXiv:1408.1670 \[hep-ph\]](#).
- [29] M. Prüfer, P. Kunkel, H. Strobelt, S. Lannig, D. Linnemann, C.-M. Schmied, J. Berges, T. Gasenzer, and M. K. Oberthaler, Observation of universal dynamics in a spinor Bose gas far from equilibrium, *Nature* **563**, 217 (2018), [arXiv:1805.11881 \[cond-mat.quant-gas\]](#).
- [30] Y.-C. Chen, C.-W. Lin, Y.-J. Lee, and P. Chang (Belle), Search for long range flow-like correlation in hadronic  $e^+e^-$  collisions with Belle, *PoS ICHEP2020*, 541 (2021).
- [31] V. Andreev *et al.* (H1), Measurement of charged particle multiplicity distributions in DIS at HERA and its implication to entanglement entropy of partons, *Eur. Phys. J. C* **81**, 212 (2021), [arXiv:2011.01812 \[hep-ex\]](#).
- [32] Z. Tu (H1, ZEUS), HERA data on azimuthal decorrelation and charged particle multiplicity spectra probing QCD dynamics and quantum entanglement effects, *PoS ICHEP2020*, 513 (2021), [arXiv:2011.02875 \[hep-ex\]](#).
- [33] Z. Tu, D. E. Kharzeev, and T. Ullrich, Einstein-Podolsky-Rosen Paradox and Quantum Entanglement at Subnucleonic Scales, *Phys. Rev. Lett.* **124**, 062001 (2020), [arXiv:1904.11974 \[hep-ph\]](#).
- [34] J. Berges, S. Floerchinger, and R. Venugopalan, Thermal excitation spectrum from entanglement in an expanding quantum string, *Phys. Lett. B* **778**, 442 (2018), [arXiv:1707.05338 \[hep-ph\]](#).
- [35] J. Berges, S. Floerchinger, and R. Venugopalan, Dynamics of entanglement in expanding quantum fields, *JHEP* **04**, 145, [arXiv:1712.09362 \[hep-th\]](#).
- [36] M. Ablikim *et al.* (BESIII), Polarization and Entanglement in Baryon-Antibaryon Pair Production in Electron-Positron Annihilation, *Nature Phys.* **15**, 631 (2019), [arXiv:1808.08917 \[hep-ex\]](#).
- [37] E. Commins and P. Bucksbaum, *Weak Interactions of Leptons and Quarks* (1983).
- [38] X.-Q. Hao, H.-W. Ke, Y.-B. Ding, P.-N. Shen, and X.-Q. Li, Testing the Bell Inequality at Experiments of High Energy Physics, *Chinese Physics C* **34**, 1 (2010), [arXiv:0904.1000](#).
- [39] A. Barr, Testing Bell inequalities in Higgs boson decays, (2021), [arXiv:2106.01377 \[hep-ph\]](#).
- [40] M. Fabbrichesi, R. Floreanini, and G. Panizzo, Testing Bell inequalities at the LHC with top-quark pairs, (2021), [arXiv:2102.11883 \[hep-ph\]](#).
- [41] N. A. Tornqvist, Suggestion for Einstein-podolsky-rosen Experiments Using Reactions Like  $e^+e^- \rightarrow \Lambda\bar{\Lambda} \rightarrow \pi^-p\pi^+\bar{p}$ , *Found. Phys.* **11**, 171 (1981).
- [42] D. Bohm, A Suggested interpretation of the quantum theory in terms of hidden variables. 1., *Phys. Rev.* **85**, 166 (1952).
- [43] D. Bohm, A Suggested interpretation of the quantum theory in terms of hidden variables. 2., *Phys. Rev.* **85**, 180 (1952).
- [44] J. F. Clauser, M. A. Horne, A. Shimony, and R. A. Holt, Proposed experiment to test local hidden-variable theories, *Phys. Rev. Lett.* **23**, 880 (1969).
- [45] M. Giustina, M. A. M. Versteegh, S. Wengerowsky, J. Handsteiner, A. Hochrainer, K. Phelan, F. Steinlechner, J. Kofler, J.-Å. Larsson, C. Abellán, W. Amaya, V. Pruneri, M. W. Mitchell, J. Beyer,

- T. Gerrits, A. E. Lita, L. K. Shalm, S. W. Nam, T. Scheidl, R. Ursin, B. Wittmann, and A. Zeilinger, Significant-Loophole-Free Test of Bell's Theorem with Entangled Photons, *Physical Review Letters* **115**, 250401 (2015).
- [46] B. Hensen, H. Bernien, A. E. Dréau, A. Reiserer, N. Kalb, M. S. Blok, J. Ruitenbergh, R. F. L. Vermeulen, R. N. Schouten, C. Abellán, W. Amaya, V. Pruneri, M. W. Mitchell, M. Markham, D. J. Twitchen, D. Elkouss, S. Wehner, T. H. Taminiau, and R. Hanson, Loophole-free Bell inequality violation using electron spins separated by 1.3 kilometres, *Nature* **526**, 682 (2015).
- [47] D. Rauch, J. Handsteiner, A. Hochrainer, J. Gallicchio, A. S. Friedman, C. Leung, B. Liu, L. Bulla, S. Ecker, F. Steinlechner, R. Ursin, B. Hu, D. Leon, C. Benn, A. Ghedina, M. Cecconi, A. H. Guth, D. I. Kaiser, T. Scheidl, and A. Zeilinger, Cosmic Bell Test Using Random Measurement Settings from High-Redshift Quasars, *Physical Review Letters* **121**, 080403 (2018).
- [48] X. H. Wu, H. S. Zong, H. R. Pang, and F. Wang, Bell inequality for Werner states, *Physical Review A - Atomic, Molecular, and Optical Physics* **64**, 3 (2001).
- [49] V. A. Andreev and V. I. Man'ko, Bell's inequality for two-particle mixed spin states, *Theoretical and Mathematical Physics* **140**, 1135 (2004).
- [50] M. B. Plenio and S. Virmani, An Introduction to entanglement measures, *Quant. Inf. Comput.* **7**, 1 (2007), [arXiv:quant-ph/0504163](https://arxiv.org/abs/quant-ph/0504163).
- [51] A. Peres, Separability criterion for density matrices, *Phys. Rev. Lett.* **77**, 1413 (1996), [arXiv:quant-ph/9604005](https://arxiv.org/abs/quant-ph/9604005).
- [52] P. Horodecki, Separability criterion and inseparable mixed states with positive partial transposition, *Phys. Lett. A* **232**, 333 (1997), [arXiv:quant-ph/9703004](https://arxiv.org/abs/quant-ph/9703004).
- [53] J. Keeling, Lectures on Quantum Magnetism, <https://www.st-andrews.ac.uk/~jmjk/keeling/teaching/magnetism-notes.pdf>, (2019).
- [54] M. Burkardt and R. L. Jaffe, Polarized  $q \rightarrow \Lambda$  fragmentation functions from  $e^+e^- \rightarrow \Lambda + X$ , *Phys. Rev. Lett.* **70**, 2537 (1993), [arXiv:hep-ph/9302232](https://arxiv.org/abs/hep-ph/9302232).
- [55] A. Moretti (COMPASS), Transversity and  $\Lambda$  polarization at COMPASS, *PoS SPIN2018*, 138 (2018), [arXiv:1901.01735 \[hep-ex\]](https://arxiv.org/abs/1901.01735).
- [56] J. R. Schrieffer and P. A. Wolff, Relation between the Anderson and Kondo Hamiltonians, *Physical Review* **149**, 491 (1966).
- [57] K. Hattori, K. Itakura, S. Ozaki, and S. Yasui, QCD Kondo effect: quark matter with heavy-flavor impurities, *Phys. Rev. D* **92**, 065003 (2015), [arXiv:1504.07619 \[hep-ph\]](https://arxiv.org/abs/1504.07619).
- [58] M. A. Ruderman and C. Kittel, Indirect exchange coupling of nuclear magnetic moments by conduction electrons, *Phys. Rev.* **96**, 99 (1954).
- [59] T. Kasuya, Theory of Metallic Ferro- and Antiferromagnetism on Zener's Model, *Progress of Theoretical Physics* **16**, 1, 45 (1956).
- [60] K. Yoshida, Magnetic Properties of Cu-Mn Alloys, *Physical Review* **106**, 893 (1957).
- [61] R. Žitko and J. Bonča, Multiple-impurity anderson model for quantum dots coupled in parallel, *Physical Review B* **74**, 10.1103/physrevb.74.045312 (2006).
- [62] F. Eickhoff and F. B. Anders, Strongly correlated multi-impurity models: The crossover from a single-impurity problem to lattice models, *Physical Review B* **102**, 10.1103/physrevb.102.205132 (2020).
- [63] K. Wilson, The renormalization group: Critical phenomena and the kondo problem, *Reviews of Modern Physics* **47**, 773 (1975).
- [64] H. R. Krishna-Murthy, J. W. Wilkins, and K. Wilson, Renormalization-group approach to the anderson model of dilute magnetic alloys. i. static properties for the symmetric case, *Physical Review* **B21**, 1003 (1980).
- [65] P. D. Sacramento and P. Schlottmann, Thermodynamics of the single-channel kondo impurity of spin  $s(\leq 7/2)$  in a magnetic field, *Phys. Rev. B* **40**, 431 (1989).
- [66] P. W. Anderson, A poor man's derivation of scaling laws for the kondo problem, *Journal of Physics C: Solid State Physics* **3**, 2436 (1970).
- [67] G. Cohen, E. Gull, D. R. Reichman, and A. J. Millis, Taming the dynamical sign problem in real-time evolution of quantum many-body problems, *Phys. Rev. Lett.* **115**, 266802 (2015).
- [68] A. Smith, M. S. Kim, F. Pollmann, and J. Knolle, Simulating quantum many-body dynamics on a current digital quantum computer, *npj Quantum Inf.* **5**, 106 (2019), [arXiv:1906.06343 \[quant-ph\]](https://arxiv.org/abs/1906.06343).
- [69] J. J. García-Ripoll, E. Solano, and M. A. Martin-Delgado, Quantum simulation of anderson and kondo lattices with superconducting qubits, *Physical Review B* **77**, 10.1103/physrevb.77.024522 (2008).
- [70] A. Asfaw, A. Corcoles, L. Bello, Y. Ben-Haim, M. Bozzorrey, S. Bravyi, N. Bronn, L. Capelluto, A. C. Vazquez, J. Ceroni, R. Chen, A. Frisch, J. Gambetta, S. Garion, L. Gil, S. D. L. P. Gonzalez, F. Harkins, T. Imamichi, H. Kang, A. h. Karamlou, R. Loredo, D. McKay, A. Mezzacapo, Z. Mineev, R. Movassagh, G. Nannicini, P. Nation, A. Phan, M. Pistoia, A. Rattew, J. Schaefer, J. Shabani, J. Smolin, J. Stenger, K. Temme, M. Tod, S. Wood, and J. Wootton., *Learn quantum computation using qiskit* (2020).
- [71] Y. Guan *et al.* (Belle), Observation of Transverse  $\Lambda/\bar{\Lambda}$  Hyperon Polarization in  $e^+e^-$  Annihilation at Belle, *Phys. Rev. Lett.* **122**, 042001 (2019), [arXiv:1808.05000 \[hep-ex\]](https://arxiv.org/abs/1808.05000).
- [72] G. Bunce *et al.*,  $\Lambda$  Hyperon Polarization in Inclusive Production by 300-GeV Protons on Beryllium., *Phys. Rev. Lett.* **36**, 1113 (1976).
- [73] K. J. Heller *et al.*, Polarization of  $\Lambda$ s and anti- $\Lambda$ s Produced by 400-GeV Protons, *Phys. Rev. Lett.* **41**, 607 (1978), [Erratum: *Phys.Rev.Lett.* 45, 1043 (1980)].
- [74] A. N. Aleev *et al.* (BIS-2), Polarization of  $\Lambda^0$  Produced by Neutrons With an Energy of Approximately 40-GeV on Carbon Nuclei, *Sov. J. Nucl. Phys.* **37**, 880 (1983).
- [75] P. Astier *et al.* (NOMAD), Measurement of the  $\Lambda$  polarization in  $\nu/\mu$  charged current interactions in the NOMAD experiment, *Nucl. Phys. B* **588**, 3 (2000).
- [76] P. Astier *et al.* (NOMAD), Measurement of the anti- $\Lambda$  polarization in muon-neutrino charged current interactions in the NOMAD experiment, *Nucl. Phys. B* **605**, 3 (2001), [arXiv:hep-ex/0103047](https://arxiv.org/abs/hep-ex/0103047).
- [77] J. Felix *et al.* (E690),  $\Lambda^0$  Polarization in 800 GeV/c  $pp \rightarrow p_f(\Lambda^0 K^+)$ , *Phys. Rev. Lett.* **88**, 061801 (2002).
- [78] M. I. Adamovich *et al.* (WA89), A measurement of  $\Lambda$  polarization in inclusive production by  $\Sigma^-$  of 340-GeV/c in C and Cu targets, *Eur. Phys. J. C* **32**, 221 (2004).

- [79] I. Abt *et al.* (HERA-B), Polarization of Lambda and anti-Lambda in 920-GeV fixed-target proton-nucleus collisions, *Phys. Lett. B* **638**, 415 (2006), [arXiv:hep-ex/0603047](#).
- [80] J. L. Sanchez-Lopez *et al.* (SELEX), Polarization of  $\Lambda^0$  and  $\bar{\Lambda}^0$  inclusively produced by 610-GeV/c  $\Sigma^-$  and 525-GeV/c proton beams (2007), [arXiv:0706.3660 \[hep-ex\]](#).
- [81] G. Agakishiev *et al.* (HADES), Lambda hyperon production and polarization in collisions of p(3.5 GeV)+Nb, *Eur. Phys. J. A* **50**, 81 (2014), [arXiv:1404.3014 \[nucl-ex\]](#).
- [82] A. Airapetian *et al.* (HERMES), Transverse Polarization of Lambda and anti-Lambda Hyperons in Quasireal Photoproduction, *Phys. Rev. D* **76**, 092008 (2007), [arXiv:0704.3133 \[hep-ex\]](#).
- [83] F. Hauenstein *et al.* (COSY-TOF), Measurement of polarization observables of the associated strangeness production in proton proton interactions, *Eur. Phys. J. A* **52**, 337 (2016), [arXiv:1607.06305 \[nucl-ex\]](#).
- [84] L. Adamczyk *et al.* (STAR), Global  $\Lambda$  hyperon polarization in nuclear collisions: evidence for the most vortical fluid, *Nature* **548**, 62 (2017), [arXiv:1701.06657 \[nucl-ex\]](#).
- [85] T. Sjöstrand, S. Mrenna, and P. Z. Skands, A Brief Introduction to PYTHIA 8.1, *Comput. Phys. Commun.* **178**, 852 (2008), [arXiv:0710.3820 \[hep-ph\]](#).
- [86] R. F. Werner, Quantum states with einstein-podolsky-rosen correlations admitting a hidden-variable model, *Phys. Rev. A* **40**, 4277 (1989).
- [87] Y. B. Band and P. A. Mello, Partial transposition in a finite-dimensional Hilbert space: physical interpretation, measurement of observables, and entanglement, *Quantum Studies: Mathematics and Foundations* **5**, 177 (2018), [arXiv:1705.09613](#).
- [88] A. Accardi *et al.*, Electron Ion Collider: The Next QCD Frontier: Understanding the glue that binds us all, *Eur. Phys. J. A* **52**, 268 (2016), [arXiv:1212.1701 \[nucl-ex\]](#).
- [89] R. Abdul Khalek *et al.*, Science Requirements and Detector Concepts for the Electron-Ion Collider: EIC Yellow Report, (2021), [arXiv:2103.05419 \[physics.ins-det\]](#).